Pr^{3+} crystal-field excitation study of apical oxygen and reduction processes in $Pr_{2-x}Ce_xCuO_{4\pm\delta}$

G. Riou,* P. Richard, S. Jandl, M. Poirier, and P. Fournier†
Centre de Recherche sur les Propriétés Électroniques des Matériaux Avancés, Département de Physique, Université de Sherbrooke, Sherbrooke, Canada J1K 2R1

V. Nekvasil
Institute of Physics, Czech Academy of Sciences, Cukrovarnická 10, 162 53 Praha 6, Czech Republic

S. N. Barilo and L. A. Kurnevich
Institute of Solid State and Semiconductors Physics, National Academy of Science, 17 P. Brovka street, Minsk 220072, Belarus
(Received 4 March 2003; revised manuscript received 10 September 2003; published 15 January 2004)

We present an infrared transmission Pr^{3+} crystal-field study of as-grown, reduced, and oxygenated $Pr_{2-x}Ce_xCuO_{4\pm\delta}$ single crystals and thin films. Excitations from the ground-state multiplet $^3H_4$ to the $^3H_5$, $^3H_6$, $^3F_2$, and $^3F_3$ excited multiplets are observed in all samples. In addition to the Pr^{3+} regular sites, which remain unperturbed following the cerium doping or the oxygen content modifications, Pr^{3+} sites are detected. A precise set of crystal-field parameters, which reproduces the energy and the symmetry of the levels, is determined. The reduction process, which drives the electron-doped cuprates superconducting, is discussed in detail and scenarios for the reduction mechanism and induced vacancies are proposed. In contrast to the common belief, the apical oxygen, which is clearly detected in all samples, is not removed in $Pr_{1.85}Ce_{0.15}CuO_4$ following reduction. This observation questions the role attributed to the apical oxygen removal in triggering the superconductivity.

DOI: 10.1103/PhysRevB.69.024511 PACS number(s): 74.72.Dn, 71.70.Ch, 71.70.Gm, 75.10.Dg

I. INTRODUCTION

Electron-doped compounds $RE_{2-x}Ce_xCuO_4$ (RE—rare-earth) become superconducting when annealed under reducing conditions that remove oxygen. A controversy still remains on which oxygen atoms are displaced during reduction, and thus on the effects of this reduction process on the appearance of superconductivity. Elastic neutron-scattering studies suggest that the reduction process removes oxygen from both oxygen planes and interstitial positions (oxygen in apical position with respect to copper ion) in Nd_2CuO_4,[1] and possibly in $Nd_{2-x}Ce_xCuO_4$.[2] Vigoureux *et al.*[3,4] reported that the reduction mechanism in undoped and Ce-doped Nd_2CuO_4 were different. They concluded that the O1 type oxygen, which is located in the CuO_2 planes, is removed in Nd_2CuO_4 while apical oxygen is released during the reduction process of $Nd_{2-x}Ce_xCuO_4$. Evidence for the presence of oxygen in the apical position has been reported in a ^{57}Co substituted $Nd_{2-x}Ce_xCuO_4$ Mössbauer study even after reduction.[5] Iodometric titration and thermogravimetric analysis indicate that only a small amount of oxygen is removed during the reduction process.[6] Moreover, the oxygen amount ''lost'' during reduction decreases as the Ce-doping increases, underlining the possible trapping of apical oxygen in proximity of the cerium ions. The oxygen stoichiometry variation being too small, and sometimes even below the detection limits of most techniques, the reduction mechanism and the oxygen stoichiometry in the $RE_{2-x}Ce_xCuO_4$ compounds remain an important open question.

RE crystal-field (CF) excitations, sensitively reflecting the local crystallographic structure, charge redistribution, and magnetic ordering, have been successfully used to study various physical properties of the high-temperature superconductors (HTSC) and their parent compounds.[7,8] Particularly, Raman scattering and infrared transmission spectroscopies have proven to be valuable techniques in the determination of the rare-earth CF excitations in both electron-doped[9–12] and hole-doped cuprates.[13,14] Since the rare-earth ions are surrounded by oxygen ions, defects such as oxygen vacancies and interstitial oxygens affect their CF energy levels. Pr^{3+} CF excitations in Pr_2CuO_4 and $Pr_{2-x}Ce_xCuO_4$ have been studied by Raman[10,12] and neutron-scattering techniques,[15] while infrared transmission spectroscopy has been limited to Pr_2CuO_4.[9] In addition to the Pr^{3+} regular site, nonregular Pr^{3+} sites of lower symmetry have been reported. Raman-scattering studies, in undoped and Ce-doped Pr_2CuO_4, have revealed the presence of the $\approx 580\ cm^{-1}$ A^* local mode associated with the characteristic structural instability of the 2-1-4 compounds.[16] The origin of this A^* mode, also extensively discussed in the literature, is not completely understood. Heyen *et al.*[17] have tentatively ascribed it to apical oxygen vibrations along the *z* axis, while Sanjuan *et al.*[18] have invoked the Ce^{4+} electronic levels in its resonance studies and Sanjuan and Laguna[16] have attributed its appearance to some degree of disorder in the oxygen sublattice.

In order to further refine our understanding of the oxygen stoichiometry effects in $Pr_{2-x}Ce_xCuO_4$ compounds and their role in the appearance of superconductivity, we present a Pr^{3+} CF infrared transmission study of $Pr_{2-x}Ce_xCuO_4$ single crystals. The main objectives are: (i) to report and fit the as-detected Pr^{3+} CF excitations for the regular sites by infrared transmission spectroscopy in order to complement the previous Pr_2CuO_4 CF studies, (ii) to discuss the origin of the

additional Pr^{3+} CF excitations in oxygenated and reduced samples, and (iii) to explain the reduction process mechanism that triggers superconductivity in $Pr_{1.85}Ce_{0.15}CuO_4$.

II. EXPERIMENTS

Infrared transmission spectra of $Pr_{2-x}Ce_xCuO_4$ ($x=0,0.03$, 0.05, 0.08, 0.11, and 0.15) single crystals and of superconducting $Pr_{1.85}Ce_{0.15}CuO_4$ thin films were measured as a function of temperature. The single crystals were grown by top-seeded solution method[19] and polished down to 70 μm along the *a* axis. The *c* oriented thin films were obtained by pulsed-laser deposition[20] with an average thickness of 3000 Å. Preliminary Raman-scattering studies have enabled us to check the orientation of the $Pr_{2-x}Ce_xCuO_4$ single crystals, prior to the infrared measurements, as well as to study their low-energy phonons and their A^* local mode. In order to study the oxygen stoichiometry effects on Pr^{3+} CF excitations, each single crystal has been measured in the as-grown, reduced, and oxygenated states. The reduction process has been performed around 900°C under an Ar flow during 36 h, the samples being sandwiched between two $Pr_{1.85}Ce_{0.15}CuO_4$ polycrystalline pellets to insure a homogenous repartition of oxygen vacancies. The oxygenation process was done in an oxygen flow at 950°C for 96 h. The samples were mounted afterwards in a continuous-flow temperature regulated helium cryostat and 0.5 cm^{-1} resolution transmission spectra were obtained in the 1800–8000 cm^{-1} energy range using a Fourier-transform interferometer (BOMEM DA3.002) equipped with a quartz source, an InSb detector and a CaF_2 beam splitter.

In order to further characterize the $Pr_{2-x}Ce_xCuO_4$ single crystals and thin films, microwave conductivity at 16.5 GHz was measured, for temperatures between 4.2 and 300 K, using the standard cavity perturbation technique.[21] This contactless technique is well suited for the measurements of electrical conductivity in highly anisotropic materials without damaging the surfaces for subsequent annealings. The reduced $Pr_{1.85}Ce_{0.15}CuO_4$ single crystal microwave conductivity at 16.5 GHz exhibits a superconducting transition around 20 K and its low *c*-axis plasma frequency, around 70 cm^{-1}, renders its infrared transmission possible for $\mathbf{E}\|\mathbf{c}$ configuration.[22]

III. RESULTS

The sample orientation was determined by Raman scattering; in the *zz* configuration, the A_{1g} phonon is detected, at 228 cm^{-1} and the E_g phonon around 475 cm^{-1}, in the as-grown $Pr_{2-x}Ce_xCuO_4$ single crystals [Fig. 1(a)]. The squiggles between 100 and 200 cm^{-1} are due to the notch filter interferences. An additional excitation, the so-called A^* local mode is also present in these spectra, around 580 cm^{-1} [Fig. 1(a)]. Upon cerium doping, an inversion of the A_{1g} and the A^* relative intensities (integrated surfaces) is observed for cerium concentrations greater than 10%. The A^* local mode is associated with a defect which is strongly enhanced by Ce^{4+} doping. Moreover, this excitation is suppressed by the reduction of Pr_2CuO_4, but remains unchanged in the

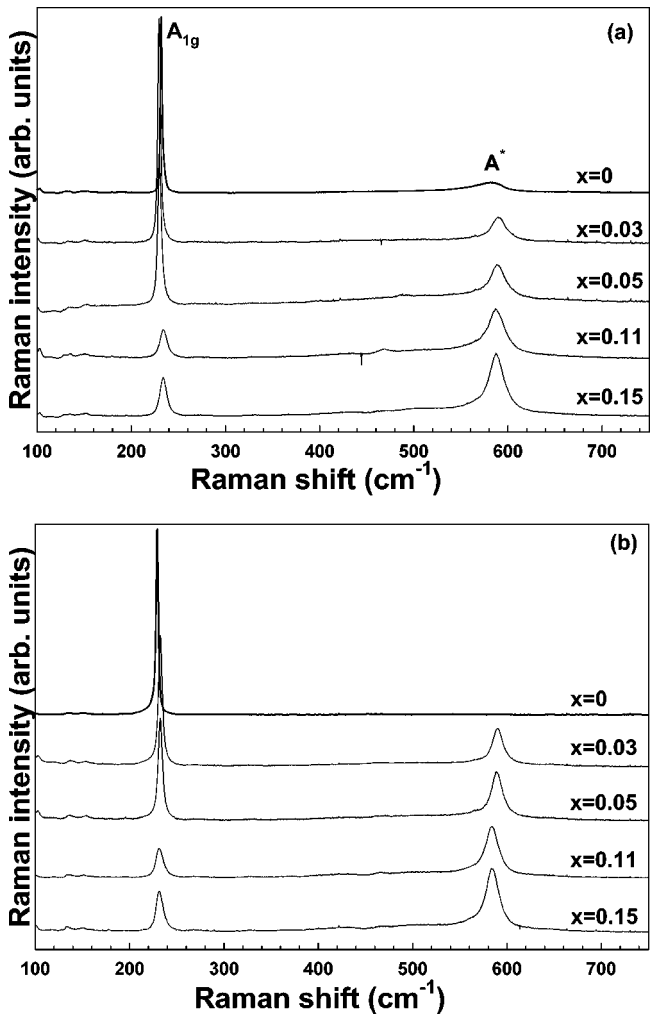

FIG. 1. The temperature evolution Raman-active excitations of as-grown (a) and reduced (b) $Pr_{2-x}Ce_xCuO_4$ single crystals in the $x(zz)\bar{x}$ configuration at 9 K.

cerium-doped compounds. This is obvious if one compares $x=0$ and $x=0.15$ spectra in Figs. 1(a) and 1(b). This implies that the A^* mode is likely due to the presence of oxygen ions in apical sites. Ce^{4+} induced local distortions would allow the incorporation of oxygen ions in apical positions and enhance the A^* mode intensities. Once oxygenated after reduction, the A^* intensity is restored to the level observed in as-grown Pr_2CuO_4, which is an indication of the apical oxygen annealing reversibility.

The C_{4v} symmetry of the crystal field at the Pr^{3+} site lifts the $(2J+1)$fold degeneracy of the J multiplets for the $4f^2$ electronic states. Assuming a perfect orientation of the crystal and the absence of depolarization effects as well as of disorder, $\Gamma_i \rightarrow \Gamma_i$ ($i=1$, 2, 3, 4, 5) dipole transitions are allowed for $\mathbf{E}\|\mathbf{c}$ while $\Gamma_5 \rightarrow \Gamma_1$, Γ_2, Γ_3, and Γ_4 dipole transitions are allowed for $\mathbf{E}\perp\mathbf{c}$.[23,12]

As was found for undoped and cerium-doped Nd_2CuO_4 and Pr_2CuO_4 crystals,[9,11] more infrared absorption bands are observed than expected from the Pr^{3+} regular sites. The additional absorption bands are due to nonregular Pr^{3+} sites,

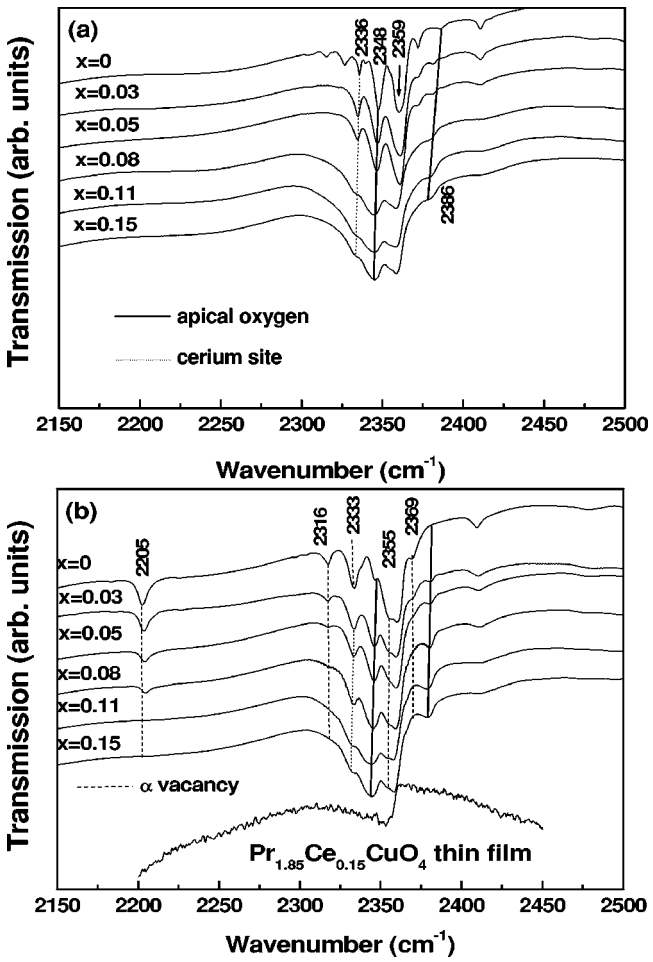

FIG. 2. As-grown (a) and reduced (b) $Pr_{2-x}Ce_xCuO_4$ single crystal cerium doping evolution, of the Pr^{3+} $^3H_4 \rightarrow {}^3H_5$ CF absorption bands for $\mathbf{E}\|\mathbf{c}$ at 9 K. A superconducting $Pr_{1.85}Ce_{0.15}CuO_4$ thin film spectrum is also presented [in (b)] for $\mathbf{E}\perp\mathbf{c}$ at 9 K. The arrow indicates Pr^{3+} regular site excitation.

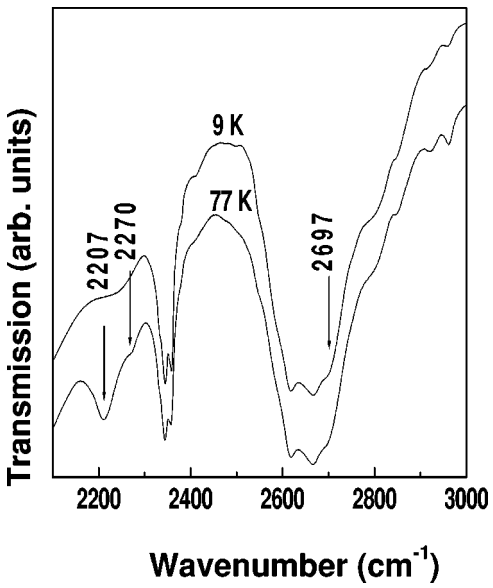

FIG. 3. $Pr_{1.85}Ce_{0.15}CuO_4$ single crystal temperature evolution of the Pr^{3+} $^3H_5$ CF absorption bands.

whose frequencies are influenced by the nature of the doping, local defects, or oxygen nonstoichiometry. Pr^{3+} CF absorption bands at 9 K are shown in Figs. 2–7. Transmission spectra for various concentrations, oxygenation and reduction have been normalized with respect to the $x=0$ spectrum. A direct comparison with a previously reported study of Pr^{3+} CF excitations in Pr_2CuO_4 (Ref. 9) allows the identification of the absorption bands associated with the Pr^{3+} CF excitations at the regular sites in undoped and cerium doped Pr_2CuO_4 compounds. Most of the Pr^{3+} regular site CF excitations reported in Ref. 9 for the undoped compound are detected and their frequencies are given for $Pr_{1.85}Ce_{0.15}CuO_4$ in Table I. The remaining absorption bands are attributed to nonregular sites. A formal fitting procedure with Gaussian curves, taking the strongest regular absorption band as reference, has been performed to compare absorption band profiles and their evolution with oxygen treatments. Among them are the absorption bands that are associated with the CF excitations in the vicinity of an oxygen vacancy or an extra oxygen in the apical position. Moreover, the intensities of the Pr^{3+} nonregular excitations associated with a particular oxygen vacancy type vary proportionally to their density. Different vacancy types may be distinguished since their CF excitation intensities do not appear in the same proportions in each sample after reduction.

The cerium doping evolution of the $^3H_4 \rightarrow {}^3H_5$ transitions is presented in Figs. 2(a) and 2(b). Taking into account the usual absorption band broadenings and small shifts in energy due to cerium doping, the as-grown $Pr_{2-x}Ce_xCuO_4$ infrared spectra display similar features as a function of cerium doping. The absorption band at 2359 cm^{-1} is associated with a $^3H_4$ $\Gamma_3 \rightarrow$ $^3H_5$ Γ_5 transition while the absorption band at 2697 cm^{-1} corresponds to a $^3H_4$ $\Gamma_3 \rightarrow$ $^3H_5$ Γ_3 transition. Absorption bands at 2207 and 2270 cm^{-1} (Fig. 3) are associated with transitions from the thermally populated 148 cm^{-1} $^3H_4$ Γ_5 first excited level to $^3H_5$ Γ_4 (2355 -148 $cm^{-1}=2207$ cm^{-1}) and $^3H_5$ Γ_2 (2418-148 cm^{-1} $=2270$ cm^{-1}) levels, respectively. In addition to absorption bands from the regular sites (indicated by downward arrows), many unexpected excitations are detected and associated with nonregular Pr^{3+} sites. The oxygen nonstoichiometry is first considered with Fig. 2(b) displaying the reduced $Pr_{2-x}Ce_xCuO_4$ infrared spectra. The intensities of the absorption bands at 2205, 2316, 2333, 2355, and 2369 cm^{-1} are enhanced by the reduction process of lightly cerium-doped compounds ($x \leqslant 0.08$) but become undetectable for higher cerium contents and in the $Pr_{1.85}Ce_{0.15}CuO_4$ thin-films spectra. This set of additional absorption bands corresponds to CF excitations of Pr^{3+} in the vicinity of oxygen vacancies. Thus the reduction process is different in undoped and cerium-doped $Pr_{2-x}Ce_xCuO_4$ samples. In Pr_2CuO_4 the absorption band intensities at 2348 and 2386 cm^{-1} decrease after oxygen reduction and increase after oxygenation (not shown). However, these absorption bands are strongly favored by cerium doping and are not affected by the reduction processes when cerium doping is present. We assign them to

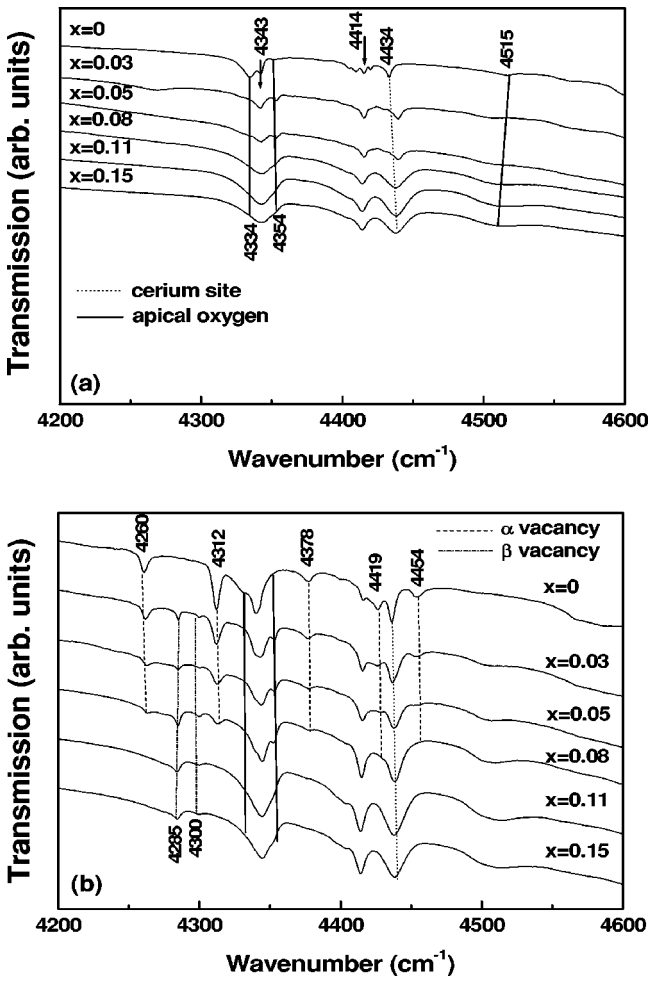

FIG. 4. As-grown (a) and reduced (b) $Pr_{2-x}Ce_xCuO_4$ single crystal cerium doping evolution of the Pr^{3+} $^3H_4 \rightarrow {}^3H_6$ CF absorption bands for $\mathbf{E}\|\mathbf{c}$ at 9 K. Arrows indicate Pr^{3+} regular sites excitations.

CF excitations of Pr^{3+} ions near apical oxygens that are removed by reduction in Pr_2CuO_4, while remaining tightly bound in Ce-doped Pr_2CuO_4. At 2336 cm^{-1} in Pr_2CuO_4, the absorption band is not influenced by the reduction or the oxygenation processes, but is enhanced and broadened by cerium doping in both the as-grown and reduced samples; it is thus associated with a defect reinforced by cerium.

The cerium doping evolution of the $^3H_4 \rightarrow {}^3H_6$ transitions is presented in Figs. 4(a) and 4(b). The absorption bands around 4414 cm^{-1} and 4992 cm^{-1} are associated with $^3H_4\ \Gamma_3 \rightarrow {}^3H_5\ \Gamma_5$ transitions, while the absorption band at 4343 cm^{-1} is associated with a $^3H_4\ \Gamma_3 \rightarrow {}^3H_5\ \Gamma_3$ transition. Absorption bands at 4266, 4473, and 4772 cm^{-1} (Fig. 5) are associated with transitions from the thermally populated 148 cm^{-1} $^3H_4\ \Gamma_5$ first excited level to $^3H_5\ \Gamma_5$ ($4414-148\ cm^{-1}=4266\ cm^{-1}$), $^3H_5\ \Gamma_5$ ($4621-148\ cm^{-1}=4473\ cm^{-1}$) and $^3H_5\ \Gamma_3$ ($4920-148\ cm^{-1}=4772\ cm^{-1}$) levels, respectively. The reduction process, as shown by the Pr^{3+} CF excitations [Fig. 4(b)], is different for Pr_2CuO_4 as compared to $Pr_{2-x}Ce_xCuO_4$. Excitations at 4260, 4312, 4378, 4419, and 4454 cm^{-1}, appearing after the reduction process in samples with $x<0.08$, vanish for higher cerium contents. On the other hand, two absorption bands at 4285 and 4300 cm^{-1} are induced by the reduction in the cerium-doped compounds. These two sets of absorption bands correspond to Pr^{3+} CF excitations near two *distinct types* of oxygen vacancies. The absorption bands at 4334, 4354 and 4515 cm^{-1} are reinforced by the oxygenation process (not shown), and suppressed after reduction in Pr_2CuO_4. They are associated with Pr^{3+} ions in the vicinity of oxygen ions in the apical positions. As mentioned above for the $^3H_4 \rightarrow {}^3H_5$ transitions, these absorptions are not affected by the reduction of the cerium-doped compounds. The absorption band at 4434 cm^{-1} is influenced only by cerium doping, similarly to the 2336 cm^{-1} absorption band.

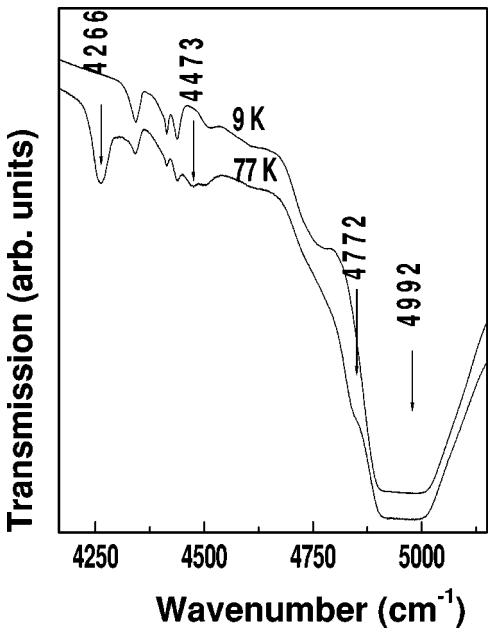

FIG. 5. $Pr_{1.85}Ce_{0.15}CuO_4$ single crystal temperature evolution of the Pr^{3+} $^3H_4 \rightarrow {}^3H_6$ CF absorption bands.

The cerium doping evolution of the $^3H_4 \rightarrow {}^3F_2$ and $^3F_3$ transitions are presented in Figs. 6(a) and 6(b). Absorption bands at 5424 cm^{-1} and 6546 cm^{-1} correspond to $^3H_4\ \Gamma_3 \rightarrow {}^3F_2\ \Gamma_5$ and $^3H_4\ \Gamma_3 \rightarrow {}^3F_3\ \Gamma_3$ transitions, respectively. High-temperature absorption bands (Fig. 7) at 5301 cm^{-1}, 6431 cm^{-1}, and 6686 cm^{-1} are associated with transitions from the thermally populated 148 cm^{-1} $^3H_4\ \Gamma_5$ level, to $^3F_3\ \Gamma_1$, $^3F_3\ \Gamma_5$, $^3F_3\ \Gamma_5$ levels respectively. The transition from the ground-state multiplet 698 cm^{-1} $^3H_4\ \Gamma_5$ level to the 6834 cm^{-1} $^3F_3\ \Gamma_5$ level corresponds to the absorption band at 6136 cm^{-1}. As previously described for the lowest frequency intermultiplet transitions, the additional absorption bands are associated with nonregular Pr^{3+} sites. The absorption band at 6847 cm^{-1}, influenced only by cerium doping, behaves like the 2336 and 4434 cm^{-1} absorption bands. Excitations at 5214, 5462, 5500, 6623, and 6693 cm^{-1}, appearing after the reduction process in samples with $x<0.08$, vanish for the higher cerium contents [Fig. 6(b)]. These additional absorption bands correspond to CF excitations of Pr^{3+} near oxygen vacancies.

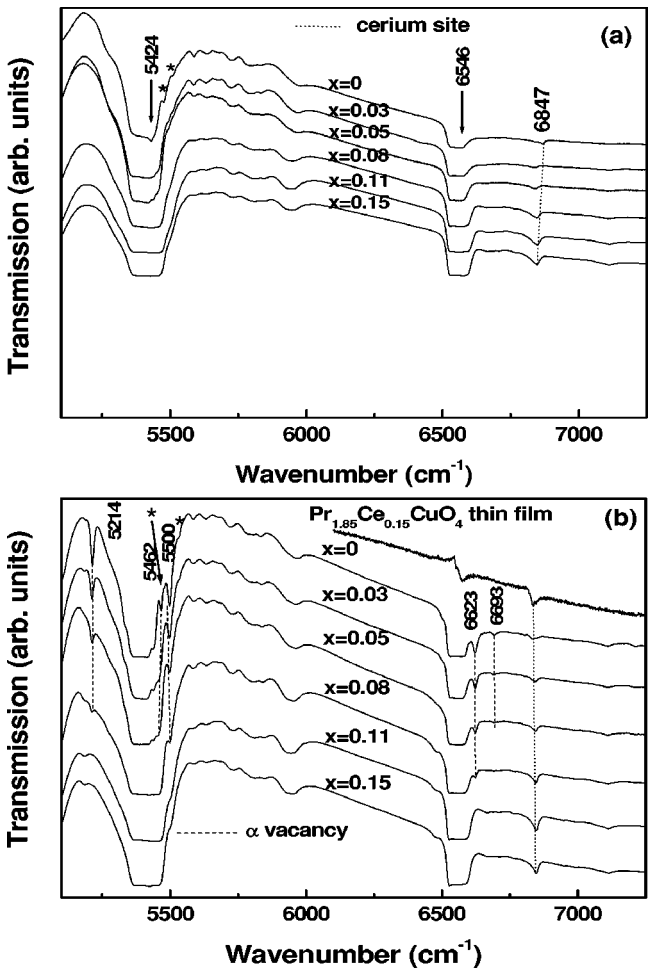

FIG. 6. As-grown (a) and reduced (b) $Pr_{2-x}Ce_xCuO_4$ single crystal cerium doping evolution of the Pr^{3+} $^3H_4 \rightarrow {}^3F_2$ and $^3F_3$ CF absorption bands for $\mathbf{E}\|\mathbf{c}$ at 9 K. A superconducting $Pr_{1.85}Ce_{0.15}CuO_4$ thin film spectrum is also presented for $\mathbf{E}\perp\mathbf{c}$ at 9 K. Arrows indicate Pr^{3+} regular sites excitations. Asterisks indicate defects that remain unaffected by the oxygenation or reduction process.

IV. DISCUSSION

A. Regular sites

A fit of the CF parameters has been performed for the regular CF levels detected in $Pr_{1.85}Ce_{0.15}CuO_4$ using the following CF Hamiltonian written with one-electron irreducible tensor operators

$$H_{CF}=\sum_{i,k,q} B_{kq}C_q^k(i), \tag{1}$$

where $C_q^k(i)$ is the qth component of a spherical tensor operator of rank k, and B_{kq} is the corresponding CF parameter. The fitting procedure is detailed in Ref. 9, and in Table II, the CF parameters for $Pr_{1.85}Ce_{0.15}CuO_4$ are given. The calculated Pr^{3+} CF level energies, using the CF parameters, compare well with the experimental observations. This indicates that the whole T′ structure[24] is conserved following the cerium doping and the five CF parameters corresponding to the Pr^{3+} regular sites in Pr_2CuO_4 (C_{4v} symmetry) reported in Ref. 9 allow the calculation of the CF levels in the cerium-doped samples within the error margins. Nevertheless, some lifting of Γ_5 degeneracies around 2362 and 4410 cm^{-1} is observed in the cerium-doped Pr_2CuO_4. This is probably due to a slight lowering of the Pr^{3+} symmetry site.

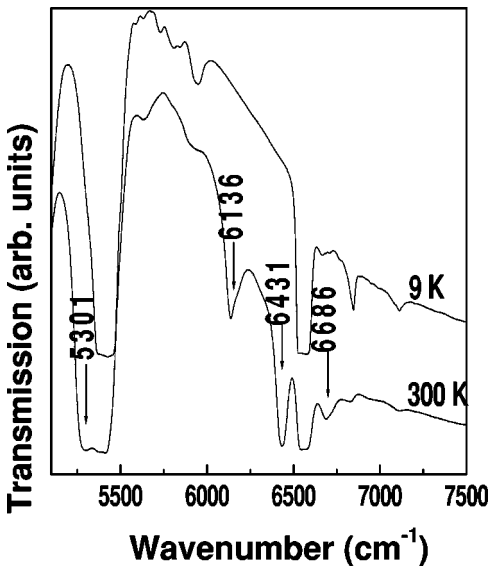

FIG. 7. $Pr_{1.85}Ce_{0.15}CuO_4$ single crystal temperature evolution of the Pr^{3+} $^3H_4 \rightarrow {}^3F_2$, and $^3F_3$ CF absorption bands.

Note that, Sanjuan *et al.*[18] have proposed that the A^* local mode could be associated with the presence of Pr^{4+} ions. In this case, Pr^{4+} crystal-field excitations are expected in the 2000–7000 cm^{-1} energy range, namely, around 2013, 2047, 3141, 5285, 5301, and 6604 cm^{-1} in $BaPrO_3$.[25] None of these absorption bands are observed in our measurements, thus excluding the presence of Pr^{4+} ions in $Pr_{2-x}Ce_xCuO_4$ compounds.

B. Nonregular sites

In addition to the regular absorption bands, additional ones are induced by cerium doping, reduction, and oxygenation processes. In Table III we tabulate the CF energy levels associated with Pr^{3+} ions located near a Ce^{4+} ion, an oxygen vacancy and an apical oxygen, respectively.

1. The cerium effect

Concerning the cerium doping reinforced inhomogeneities, two distinct scenarios have been proposed. The first one related to the refinement of the pair density function,[26] obtained from neutron powder diffraction data, shows that the CuO_2 planes are quite inhomogeneous with a distribution of undistorted and distorted domains whose origin is not explained by steric arguments (i.e., the distortion does not take place in the close proximity of the dopant ions). The second scenario reported by Allenspach *et al.*[27] invokes static phase separation into local regions of doped and antiferromagnetic character, respectively. In order to better understand the influence of cerium, we have measured the temperature evolution of the $Pr_{2-x}Ce_xCuO_4$ single crystal microwave conduc-

TABLE I. The crystal-field levels determined for the Pr^{3+} ion in regular lattice sites (in cm^{-1}) in $Pr_{1.85}Ce_{0.15}CuO_4$ as observed experimentally and predicted by the CF parameters.

Multiplet	$i(\Gamma_i)$	Experiment $Pr_{1.85}Ce_{0.15}CuO_4$	Theory $Pr_{1.85}Ce_{0.15}CuO_4$
$^3H_4$	3	0	−1
	5	148	144
	1		626
	4		695
	5	698	703
	2		761
	1		795
$^3H_5$	4	2355	2350
	5	2359	2359
	2	2418	2415
	1		2543
	3	2697	2698
	5		2755
	2		2771
	5		2838
$^3H_6$	3	4343	4349
	1		4398
	5	4414	4415
	2		4593
	5	4621	4627
	4		4918
	3	4920	4920
	5	4992	4981
	1		4990
	4		5058
$^3F_2$	3		5384
	5	5424	5429
	1	5449	5444
	4		5466
$^3F_3$	3	6546	6547
	5	6579	6568
	5	6834	6826
	2		6836
	4		7025

tivity at 16.5 GHz (Fig. 8). The Pr_2CuO_4 microwave conductivity behaves in a semiconducting fashion from 150 K up to room temperature, following the functional form $\exp(-E_a/k_bT)$ with $E_a = 0.32$ eV.[9] Below 150 K, the carriers are frozen and only a hopping conductivity regime remains possible. The $Pr_{2-x}Ce_xCuO_4$ single crystal conductivity gradually increases with cerium content, and, as expected, the highest doped compounds become more conducting.

We note that the CF excitation frequencies of the Pr^{3+} irregular cerium dependent sites are not affected by temperature above and below T_c (in $Pr_{1.85}Ce_{0.15}CuO_4$, $T_c = 22$ K). Nevertheless contrary to Nd^{3+} CF infrared transmission study in $La_{2-x-y}Nd_xSr_yCuO_4$,[28] where stripes are observed[29] and where CF excitations of Nd^{3+} ions in the metallic regions are sensitive to the charge densities, no important CF excitation frequency shifts are observed as the cerium content and conductivities increase. Consequently, we associate this site with static local distortions, and we propose that the nature of metallization in $Pr_{2-x}Ce_xCuO_4$ and $La_{2-x-y}Nd_xSr_yCuO_4$ are probably different.

TABLE II. The crystal-field parameters determined for the Pr^{3+} ion in regular lattice sites (in cm^{-1}). The mean errors associated with the fitting are shown in brackets.

CF parameters	$Pr_{1.85}Ce_{0.15}CuO_4$
B_{20}	−335(2)
B_{40}	−2328(4)
B_{44}	1953(2)
B_{60}	151(3)
B_{64}	1444(3)

2. The oxygen vacancies

The reduction process strongly depends on the cerium content. Actually, two different sets of Pr^{3+} CF excitations can be associated with the appearance of oxygen vacancies during reduction. The first set, (α type oxygen vacancy), is detected only in $Pr_{2-x}Ce_xCuO_4$ single crystals (with $x \leqslant 0.08$), while the second one (β type oxygen vacancy) is detected only in cerium-doped Pr_2CuO_4 samples (Table III). The T′ structure accommodates two oxygen types: (O1) in the copper oxygen planes and (O2) in the oxygen planes. A calculation of the Madelung potentials at O1 and O2 sites has shown that the removal of O2 oxygen is easier in Pr_2CuO_4.[30] Moreover, the repulsion between O2 oxygen ions, resulting from the lattice mismatch between the two sublattices of PrO and CuO_2, tends also to destabilize O2 pairs. Thus one could associate the α-type oxygen vacancies with O2 vacancies. The β-type vacancy is detected only in

TABLE III. The energies (in cm^{-1}) of the Pr^{3+} ^3H and ^3F term levels in $Pr_{2-x}Ce_xCuO_4$ associated with nonregular sites close to cerium, α and β vacancies, and apical oxygen (± 1 cm^{-1}).

	Cerium site	α vacancy	β vacancy	Apical oxygen
$^3H_5$	2336	2205		
		2316		
		2333		2348
		2355		2386
		2369		
$^3H_6$	4434	4260	4285	4334
		4312	4300	4354
		4378		
		4419		
		4454		4515
$^3F_2$		5214		
		5462		
		5500		
$^3F_3$	6847	6623		
		6693		

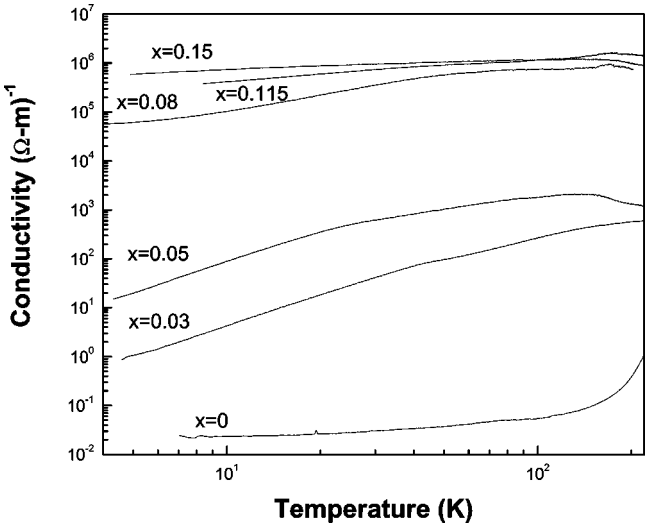

FIG. 8. The microwave conductivity of as-grown $Pr_{2-x}Ce_xCuO_4$ at 16.5 GHZ as a function of temperature on a log-log scale.

the cerium-doped samples. This observation contrasts with the report of Brinkmann *et al.*[31] that deduces indirectly the absence of vacancies in reduced $Pr_{1.85}Ce_{0.15}CuO_4$ samples from transport properties. As shown by Vigoureux *et al.*,[3,4] and theoretically demonstrated by Hirsch,[30] the reduction mechanism is clearly influenced by cerium doping.[32] However, the hypothesis that O2 type oxygens (in PrO layers) in the vicinity of cerium are released by the reduction process is not verified. A calculation performed by Whangbo *et al.*[33] proved that Cu-O bonds have antibonding character in the CuO_2 layer x^2-y^2 bands. The substitution of Pr^{3+} by Ce^{4+} corresponds to the injection of electrons in these antibonding orbitals and, consequently, in the stretching of the in-plane Cu-O and Cu-Cu bond lengths. Variations of the lattice parameters consistent with these results have been observed by Kawashima *et al.*[34] Hence, following the cerium doping the lattice parameter mismatch of the two sublattices ($Pr_{2-x}Ce_xO$ and CuO_2) is reduced, and it becomes easier to remove O(1) oxygen ions by the reduction process. We thus associate the β type oxygen defects with the O1 vacancies.

Concerning the role of the reduction process, we refer to the relative abilities of holes and electrons to suppress long-range antiferromagnetic interactions, with the magnetic frustration induced by hole doping being far more effective, than the dilution of the magnetic interaction as induced by the electron doping.[35] According to Luke *et al.*,[36] in as-grown electron-doped cuprates, magnetic ordering is seen for $x=0.14$ as high as $T=80$ K, while the reduction dramatically suppresses the magnetism. It is likely that the removal of the O1 oxygens of the CuO_2 planes destroys the long-range antiferromagnetic order and induces consequently superconductivity.

3. The apical oxygens

As mentioned previously, the absorption bands associated with Pr^{3+} CF excitations close to an interstitial oxygen are clearly identified in the Pr_2CuO_4 spectra. Unfortunately, not enough structural data are available to perform a precise prediction of the CF parameters of the Pr^{3+} ion close to an apical oxygen. Contrary to previous reports,[37] the apical oxygens are not removed by conventional thermal treatments in the cerium-doped compounds. This is evidenced by the persistence, in spite of reduction, of the 580 cm^{-1} Raman active local mode, and of the numerous infrared absorption bands as tabulated in the third column of the Table III. Actually, cerium and apical oxygen would form pairs that inject holes in the copper-oxygen planes, as reported by Chechersky *et al.*,[38] and observed in Hall effect measurements.[39]

V. CONCLUSIONS

We present in this paper a Pr^{3+} CF infrared absorption study in $Pr_{2-x}Ce_xCuO_4$ as a function of cerium doping, oxygenation, and reduction. CF levels of the first five excited multiplets have been observed. In addition to the C_{4v} symmetry regular sites, nonregular sites for Pr^{3+} have been detected in $Pr_{2-x}Ce_xCuO_4$ single crystals and thin films, while Pr^{4+} ions are absent. The detection of Pr^{3+} excitations induced by the presence of oxygen in apical positions in reduced cerium-doped Pr_2CuO_4 leads to the conclusion that the Ce^{4+} ions prevent their removal by usual reduction processes. In undoped Pr_2CuO_4, O2 oxygen ions in the oxygen planes are released by the reduction. In cerium-doped Pr_2CuO_4, the reduction removes O1 oxygen ions from the CuO_2 planes which destroys long-range antiferromagnetic interactions, and triggers superconductivity.

ACKNOWLEDGMENTS

We thank J. Rousseau, M. Castonguay, and I. Hetel for technical assistance and Dr. S.V. Shiryaev for x-ray fluorescent analysis of the $Pr_{2-x}Ce_xCuO_4$ crystal compositions. G.R., P.R., S.J., M.P., and P.F. acknowledge support from the National Science and Engineering Research Council of Canada, the Fonds Québécois de la Recherche sur la Nature et les Technologies, and The Canada Foundation for Innovation. The work in Minsk was supported in part by SNSF SCOPES program under Grant No. 7BYPJ65732. V.N. gratefully acknowledges the Grant Agency of the Czech Republic (GACR) for its grant, Grant No. 202/03/0552.

*Electronic address: griou@physique.usherb.ca
†Also at The Canadian Institute for Advanced Research.

[1] P.G. Radaelli, J.D. Jorgensen, A.J. Schultz, J.L. Peng, and R.L. Greene, Phys. Rev. B **49**, 15 322 (1994).
[2] A.J. Schultz, J.D. Jorgensen, J.L. Peng, and R.L. Greene, Phys. Rev. B **53**, 5157 (1996).
[3] P. Vigoureux, W. Paulus, M. Braden, A. Cousson, G. Heger, J.Y. Henry, V. Kvardakov, A. Ivanov, and P. Galez, Physica C **235-240**, 1263 (1994).
[4] P. Vigoureux, W. Paulus, J.Y. Henry, S. Pinol, and G. Heger, Physica C **234-236**, 719 (1997).
[5] A. Nath, N.S. Kopelev, V. Chechersky, J.L. Peng, R.L. Greene, O.

Beom-hoan, M.I. Larkin, and J.T. Markert, Science **265**, 73 (1994).
[6] P.W. Klamut, J. Alloys Compd. **194**, 15 (1993); Y. Idemoto and K. Fueki, Jpn. J. Appl. Phys. **30**, 2471 (1991).
[7] P. Allenspach, A. Furrer, F. Fauth, M. Guillaume, W. Hengeler, J. Mesot, and S. Rosenkranz, Physica B **213-214**, 78 (1995).
[8] U. Staub and L. Soderholm, in *Handbook on the Physics and Chemistry of Rare Earths*, edited by K.A. Schneidner, Jr., L. Eyring, and M.B. Maple (Elsevier, Amsterdam, 2000), Vol. 30, p. 491.
[9] G. Riou, S. Jandl, M. Poirier, V. Nekvasil, M. Diviš, P. Fournier, R.L. Greene, D.I. Zhigunov, and S.N. Barilo, Eur. Phys. J. B **23**, 179 (2001).
[10] S. Jandl, T. Strach, T. Ruf, M. Cardona, V. Nekvasil, D.I. Zhigunov, S.N. Barilo, and S.V. Shiryaev, Physica C **322**, 87 (1999).
[11] S. Jandl, P. Richard, M. Poirier, V. Nekvasil, A.A. Nugroho, A.A. Menovsky, D.I. Zhigunov, S. N Barilo, and S.V. Shiryaev, Phys. Rev. B **61**, 12 882 (2000).
[12] S. Jandl, T. Strach, T. Ruf, M. Cardona, V. Nekvasil, M. Iliev, D.I. Zhigunov, S.N. Barilo, and S.V. Shiryaev, Phys. Rev. B **56**, 5049 (1997).
[13] A.A. Martin, T. Ruf, M. Cardona, S. Jandl, D. Barba, V. Nekvasil, M. Diviš, and T. Wolf, Phys. Rev. B **59**, 6528 (1999).
[14] D. Barba, S. Jandl, V. Nekvasil, M. Maryško, M. Diviš, A. A Martin, C.T. Lin, M. Cardona, and T. Wolf, Phys. Rev. B **63**, 054528 (2001).
[15] C.-K. Loong and L. Soderholm, Phys. Rev. B **48**, 14 001 (1993).
[16] M.L. Sanjuán and M.A. Laguna, Phys. Rev. B **52**, 13 000 (1995).
[17] E.T. Heyen, R. Liu, M. Cardona, S. Pinol, R.J. Melville, D.McK. Paul, E. Moràn, and M.A. Alario-Franco, Phys. Rev. B **43**, 2857 (1991).
[18] M.L. Sanjuán, M.A. Laguna, S. Piñol, P. Canfield, and Z. Fisk, Phys. Rev. B **46**, 8683 (1992).
[19] S.N. Barilo, A.P. Ges, S.A. Guretskil, D.I. Zhigunov, A.M. Luginets, S.V. Shiryaev *et al.*, Proceedings ICMC90 Garmisch-Partenkirchen, Germany, May 9–11 (1990), p. 239.
[20] E. Maiser, P. Fournier, J.L. Peng, F.M. Araujo-Moreira, T. Venkatesan, R.L. Greene, and G. Czjzek, Physica C **297**, 15 (1998).
[21] L.I. Buranov and I.F. Schegolev, Prib. Tekh. Eksp. **2**, 171 (1971).
[22] K. Tamasaku, Y. Nakamura, and S. Uchida, Phys. Rev. Lett. **69**, 1455 (1992).
[23] The Γ_i's represent the irreducible representations of the C_{4v} point group.
[24] P. Dufour, S. Jandl, C. Thomsen, M. Cardona, B.M. Wanklyn, and C. Changkang, Phys. Rev. B **51**, 1053 (1995).
[25] M.N. Popova, B.Z. Malkin, L.A. Kasatkina, G. Cao, and J. Crow, Phys. Rev. A **223**, 308 (1996).
[26] S.J.L. Billinge and T. Egami, Phys. Rev. B **47**, 14 386 (1993).
[27] P. Allenspach, A. Furrer, F. Fauth, M. Guillaume, W. Henggeler, J. Mesot, and S. Rosenkranz, Physica C **213-214**, 78 (1995).
[28] G. Riou, S. Jandl, M. Poirier, V. Nekvasil, M. Maryško, J. Fábry, K. Jurek, M. Diviš, J. Hölsä, I.M. Sutjahja, A.A. Menovsky, S.N. Barilo, S.V. Shiryaev, and L.N. Kurnevich, Phys. Rev. B **66**, 224508 (2002).
[29] M. Roepke, E. Holland-Moritz, B. Büchner, H. Berg, R.E. Lechner, S. Longeville, J. Fitter, R. Kahn, G. Coddens, and M. Ferrand, Phys. Rev. B **60**, 9793 (1999).
[30] J.E. Hirsch, Physica C **243**, 319 (1995).
[31] M. Brinkmann, T. Rex, M. Stief, H. Bach, and K. Westerholt, Physica C **269**, 76 (1996).
[32] W. Henggeler, T. Chattopadhyay, B. Roessli, P. Vorderwisch, P. Thalmeier, D.I. Zhigunov, S.N. Barilo, and A. Furrer, Phys. Rev. B **55**, 1269 (1997).
[33] M.-H. Whangbo, M. Evain, M. Beno, and J.M. Williams, Physica C **26**, 1829 (1987).
[34] T. Kawashima and E. Takayana-Muromachi, Physica C **219**, 389 (1994).
[35] T.R. Thurston, M. Matsuda, K. Kakurai, K. Yamada, Y. Endoh, R.J. Birgeneau, P.M. Gehring, Y. Hidaka, M.A. Kastner, T. Murakami, and G. Shirane, Phys. Rev. Lett. **65**, 263 (1990).
[36] G.M. Luke, L.P. Le, B.J. Sternlieb, Y.J. Uemura, J.H. Brewer, R. Kadono, R.F. Kiefl, S.R. Kreitzman, T.M. Riseman, C.E. Stronach, M.R. Davis, S. Uchida, H. Takagi, Y. Tokura, Y. Hidaka, T. Murakami, J. Gopalakrishnan, A.W. Sleight, M.A. Subramanian, E.A. Early, J.T. Markert, M.B. Maple, and C.L. Seaman, Phys. Rev. B **42**, 7981 (1990).
[37] J.M. Tarascon *et al.*, Physica C **162**, 285 (1989); E. Takayama-Muromachi, *ibid.* **159**, 634 (1989).
[38] V. Chechersky, N.S. Kopelev, O. Beom-hoan, M.I. Larkin, J.L. Peng, J.T. Markert, R.L. Greene, and A. Nath, Hyperfine Interact. **93**, 1721 (1994).
[39] P. Fournier, P. Mohanty, E. Maiser, S. Darzens, T. Venkatesan, C. J Lobb, G. Czjzek, R.A. Webb, and R.L. Greene, Phys. Rev. Lett. **81**, 4720 (1998).